Transition Met Chem
DOI 10.1007/s11243-016-0069-9

Antioxidant and antimicrobial properties of nickel(II), cobalt(III), and zinc(II) complexes of a Schiff base ligand

Qi-Meige Hasi[1,2] · Yan Fan[1,2] · Xiao-Xia Feng[1,2] · Xiao-Qiang Yao[1,2] · Jia-Cheng Liu[1,2]

Received: 15 March 2016 / Accepted: 1 June 2016

Abstract A series of mononuclear Ni(II), Co(III), and Zn(II) complexes based on a Schiff base ligand, 4-chloro-6-[2-(pyrazin-2-ylmethylene)hydrazinyl]pyrimidine (HL), have been synthesized and characterized by physicochemical and spectroscopic methods. The complexes were found to have superior radical scavenging potency against DPPH, superoxide anion, hydroxyl, and ABTS radicals than free HL. The antibacterial effects of the complexes against Gram-positive and Gram-negative bacteria were also higher than that of free HL.

Introduction

Free radicals are involved in the processes of normal oxygen metabolism in the human body, including electron transfer in the mitochondrial respiratory chain, cell differentiation, immune response, and vasodilatation. An imbalance between formation and detoxification of free radical species results in oxidative stress. This condition can cause serious damage to proteins, lipids, and DNA, potentially leading to the development of serious diseases, e.g., some types of neoplasia, inflammation processes, and atherosclerosis [1–9]. In addition, microbial infections, in particular those caused by bacteria, remain a primary reason for mortality and morbidity all over the world [10]. Therefore, there is an impetus to search for new metal complexes which possess both antioxidant and antimicrobial activities.

Schiff base metal complexes have aroused considerable attention due to their wide biological activity, which can include antibacterial, antioxidant, and antitumor properties [11–15]. It is well known that some drugs have higher activities when administered as metal complexes compared to the free ligand [16]. Given these considerations, in this work we have synthesized a new Schiff base ligand, 4-chloro-6-[2-(pyrazin-2-ylmethylene)hydrazinyl]pyrimidine (HL, Scheme 1), and some of its metal complexes. Furthermore, the biological properties of the free ligand and its metal complexes have been investigated.

Experimental

Materials and measurements

All chemicals and solvents were commercial products and used without further purification. Elemental analyses for C, H, and N were obtained on a Vario EL instrument. ^{1}H NMR spectra were recorded on a Varian Mercury Plus-400 spectrometer, in DMSO, at 400 MHz. ^{13}C NMR spectra were measured on a Varian Mercury Plus-400 spectrometer, in DMSO, at 100 MHz. FTIR spectra were recorded in the range 4000–400 cm^{-1} on an FTS 3000 (United States DIGILAB) spectrometer using KBr pellets. Thermogravimetric analysis (TGA) experiments were carried out on a PerkinElmer TG-7 analyzer, heating from 25 to 800 °C at a

Electronic supplementary material The online version of this article (doi:10.1007/s11243-016-0069-9) contains supplementary material, which is available to authorized users.

✉ Jia-Cheng Liu
jcliuchem@163.com

[1] College of Chemistry and Chemical Engineering, Northwest Normal University, Lanzhou 730070, People's Republic of China

[2] State Key Laboratory of Coordination Chemistry, Nanjing University, Nanjing 210093, People's Republic of China

Published online: 09 June 2016

Scheme 1 Synthesis of HL. **a** Hydrazine, triethylamine, dioxane, yield 70.8 %. **b** 1-(Pyrazin-2-yl) ethanone, acetic acid, MeOH, yield 86.3 %

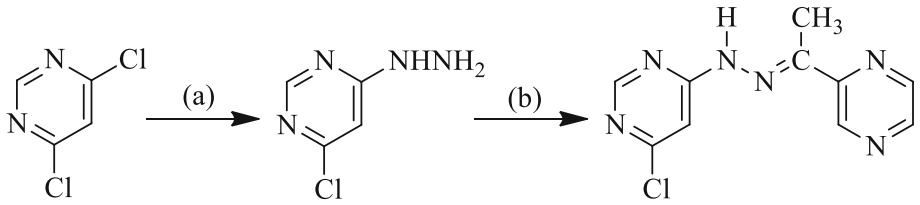

rate of 10 °C/min under N_2 atmosphere. Powder X-ray diffraction (PXRD) patterns were obtained on a Philips PW 1710 − BASED diffractometer at 293 K.

Single-crystal X-ray studies

Single-crystal X-ray diffraction analyses of complexes **1–5** were carried out on a Bruker Smart Apex CCD area detector diffractometer with graphite-monochromated Mo Kα radiation (λ = 0.71073 Å) at 296 K using the ω-scan technique. The structures were solved by direct methods and refined with the full-matrix least-squares technique using the SHELXL-97 software package. All of the non-hydrogen atoms were refined anisotropically, and all the hydrogen atoms were fixed geometrically at calculated distances and refined isotropically to ride on the parent atoms. The detailed crystallographic data and structure refinements of complexes **1–5** are given in Table 1. Selected bond lengths (Å) and angles (°) are given in Tables S1–S5.

Synthesis of HL

A stirred solution of 1-(pyrazin-2-yl)ethanone (1.24 g, 0.01 mol) in methanol (20 ml) was added dropwise to a solution of 4-chloro-6-hydrazinylpyrimidine (1.44 g, 0.01 mol) in methanol (30 ml) plus three drops of glacial acetic acid. The mixture was refluxed for 4 h and then cooled to room temperature. The precipitated solid was filtered off and washed with cold methanol to obtain a white solid. Yield: 86.3 %. ^{1}H NMR (400 MHz, DMSO) δ_{ppm}: 11.16 (s, 1H), 8.62–8.53 (m, 5H), 9.46 (s, 1H), 7.48 (s, 1H), 2.40 (s, 3H). (Fig. S1). ^{13}C NMR (100 MHz, DMSO) δ_{ppm}: 162.94, 159.80, 158.21, 150.26, 148.14,

Table 1 Crystal data and structure refinement for complexes **1–5**

Complex	**1**	**2**	**3**	**4**	**5**
Empirical formula	$C_{20}H_{16}Cl_2N_{12}Ni$	$C_{40}H_{17}Cl_8Co_3N_{24}$	$C_{20}H_{16}Cl_2N_{12}Zn$	$C_{20}H_{18}Cl_2N_{12}NiO$	$C_{20}H_{17}Cl_2CoN_{13}O_3$
Formula weight	554.04	1311.30	560.74	572.05	617.30
Temperature (K)	296 (2)	296 (2)	296 (2)	292 (2)	293 (2)
Cryst system	Monoclinic	Monoclinic	Triclinic	Monoclinic	Triclinic
Space group	*C2/c*	*C2/c*	*P*$\bar{1}$	$P2_1/n$	*P*$\bar{1}$
a (Å)	18.298 (3)	14.2644 (13)	9.6768 (13)	12.4971 (3)	8.9761 (8)
b(Å)	9.914 (2)	11.4471 (9)	10.3560 (13)	13.2900 (4)	9.0478 (9)
c(Å)	14.088 (3)	31.543 (4)	14.7389 (19)	14.2246 (4)	17.4887 (14)
α (deg)	90	90	89.612 (11)	90	75.277 (8)
β (deg)	101.47 (2)	93.346 (12)	73.026 (12)	98.318 (2)	80.196 (7)
γ (deg)	90	90	67.330 (12)	90	65.445 (9)
V (Å^3)	2504.6 (9)	5141.8 (9)	1294.2 (3)	2337.66 (11)	1246.1 (2)
Z	4	4	2	4	2
D_c (g/cm^3)	1.469	1.694	1.439	1.625	1.645
F(000)	1128.0	2636.0	568.0	1168.0	626.0
θ min, max(deg)	0.736,0.791	0.986,1.000	0.741,0.867	0.912,0.946	0.878, 0.9021
GOF	1.051	1.044	1.021	1.068	1.032
R_1 $[I > 2\sigma(I)]$[a]	0.0548	0.0533	0.0471	0.0347	0.0590
	(1640)	(3535)	(3920)	(3693)	(4066)
wR_2^b (all data)	0.1324	0.1090	0.1364	0.0881	0.1792
	(2364)	(5062)	(5066)	(4596)	(5055)

[a] $R_1 = \Sigma||F_o| - |F_c||/\Sigma|F_o|$

[b] $wR_2 = [\Sigma w(F_o^2 - F_c^2)^2/\Sigma w(F_o^2)^2]^{1/2}$

143.83, 143.13, 142.63, 102.99, 11.91. (Fig. S2). ESI–MS (DMF, positive ion mode): m/z = 249.07($[M + H]^+$), $C_{10}H_9ClN_6$ theoretical mass: 248. (Fig. S3). IR/cm^{-1} (KBr):1565 (s), 1369 (m), 3150 (m), 3438 (m).

Synthesis of $[Ni(L)_2]$ (1)

A methanol solution (10 ml) of $Ni(OAc)_2{\cdot}4H_2O$ (24.9 mg, 0.1 mmol) was added to a methanol solution (10 ml) of HL (24.8 mg, 0.1 mmol). The resulting solution was stirred for 15 min at room temperature, then filtered, and evaporated slowly to give dark green crystals after 2 weeks. Yield: 57.2 %. Anal. Calcd. For $C_{20}H_{16}Cl_2N_{12}Ni$: C, 43.4; H, 2.9; N, 30.3 %. Found: C, 43.3; H, 2.9; N, 30.3 %. IR/cm^{-1} (KBr):1559 (s), 1441(s), 1585 (m), 3438 (m).

Synthesis of $\{[Co(L)(HL)]CoCl_4\}$ (2)

An ethanol solution (10 ml) of $CoCl_2{\cdot}6H_2O$ (23.8 mg, 0.1 mmol) was added to an ethanol solution (10 ml) of HL (24.8 mg, 0.1 mmol). Green crystals were obtained by slow evaporation of the resulting solution within 5 days in 49.8 % yield. Anal. Calcd. For $C_{40}H_{34}Cl_8Co_3N_{24}$: C, 36.6; H, 2.6; N, 25.6 %. Found: C, 36.6; H, 2.6; N, 25.6 %. IR/cm^{-1} (KBr): 1598 (s), 2920 (m), 3444 (m).

Synthesis of $[Zn(L)_2]$ (3)

The preparation of complex **3** was similar to that of **2**, except that $Zn(OAc)_2$ (18.3 mg, 0.1 mmol) was used instead of $CoCl_2{\cdot}6H_2O$. Yellow crystals were obtained by slow evaporation of the resulting solution within two weeks in 55.6 % yield. Anal. Calcd. For $C_{20}H_{16}Cl_2N_{12}Zn$: C, 42.8; H, 2.9; N, 30.0 %. Found: C, 42.9; H, 2.9; N, 30.0 %. IR/cm^{-1} (KBr):1565 (s), 1435 (s), 1605 (m), 3438(m).

Synthesis of $\{[Ni(L)_2]H_2O\}$ (4)

Complex **4** was also prepared by the same method as of **2**, but using $Ni(OAc)_2{\cdot}4H_2O$ (24.9 mg, 0.1 mmol) instead of $CoCl_2{\cdot}6H_2O$. Dark green crystals were obtained by slow evaporation of the resulting solution within three weeks in 59.2 % yield. Anal. Calcd. For $C_{20}H_{18}Cl_2N_{12}NiO$: C, 42.0; H, 3.2; N, 29.4 %. Found: C, 42.0; H, 3.1; N, 29.4 %. IR/cm^{-1} (KBr):1560 (s), 1438 (s), 1353 (m), 3375 (m).

Synthesis of $\{[Co(L)_2]NO_3\}$ (5)

The preparation of complex **5** was similar to that of **2**, except that $Co(NO_3)_2{\cdot}6H_2O$ (29.1 mg, 0.1 mmol) was used instead of $CoCl_2{\cdot}6H_2O$. Red-brown crystals were obtained by slow evaporation of the resulting solution within 3 weeks in 60.2 % yield. Anal. Calcd. For $C_{20}H_{17}Cl_2CoN_{13}O_3$: C, 38.9; H, 2.8; N, 29.5 %. Found: C, 38.9; H, 2.7; N, 29.4 %. IR/cm^{-1} (KBr):1441 (s), 1565 (s), 1598 (s), 3432 (m).

Antioxidant assays

The antioxidant properties of free HL and its metal complexes were determined by DPPH radical, superoxide radical, hydroxyl radical, and ABTS radical scavenging methods. The DPPH (2,2-diphenyl-2-picryl-hydrazyl) radical scavenging activities of the test compounds were assayed using the method of Elizabeth [17], with slight modifications. Each test compound was dissolved in DMSO, and the solution of DPPH was prepared in methanol. The reaction mixture contained 2 ml of 0.2 mM DPPH solution and 100 µl of the test compound solution (the final concentration: $C_{i(i=1-5)} = 5, 10, 15, 20, 25$ µM). The reaction mixtures were incubated at 37 °C for 20 min in the dark. The decrease in absorbance of DPPH was measured at 517 nm every 5 min. As a control, the absorbance of a blank solution of DPPH (2 ml) was also determined at 517 nm. The suppression ratio was calculated by the following equation:

$$\text{Suppression ratio}\,(\%) = [(A_0 - A_i)/(A_0)] \times 100\,\%$$

where A_i = the absorbance in the presence of the test compound and A_0 = the absorbance in the absence of the test compound.

The hydroxyl radical scavenging activities of the test compounds were investigated using the Fenton reaction [18]. Each test compound was dissolved in DMF and then added to a reaction mixture containing 2.0 ml of 100 mmol phosphate buffer (pH 7.4), 1.0 ml of 0.10 mmol safranine, 1 ml of 1.0 mmol EDTA-Fe(II), and 1 ml of 3 % H_2O_2. The resulting mixtures were incubated at 37 °C for 60 min in the dark, and then the absorbance was measured at 520 nm (A_i, A_0, A_c). The suppression ratio was calculated by the following equation:

$$\text{Suppression ratio}\,(\%) = [(A_i - A_0)/(A_c - A_0)] \times 100\,\%$$

where A_i = the absorbance in the presence of the test compound; A_0 = the absorbance in the absence of the test compound; and A_c = the absorbance in the absence of the test compounds, EDTA-Fe(II) and H_2O_2.

The superoxide radical scavenging activities of the test compounds were measured using the standard testing system of NBT/$VitB_2$/MET [19]. Solutions of the test compounds were prepared in DMF. The reaction mixture contained 2.5 ml of 100 mmol phosphate buffer (pH 7.8), 1.0 ml of 50 mmol MET, 1.0 ml of 0.23 mmol NBT, 0.5 ml of 33 µM $VitB_2$, and the test compound. The solutions of MET, $VitB_2$, and NBT were prepared with phosphate buffer (pH 7.8) in the dark. After incubating the

mixture at 30 °C for 10 min and illuminating with a fluorescent lamp for 3 min, the absorbances (A_i) of the samples were measured at 560 nm. A sample without any test compound was used as the control. The suppression ratio was calculated according to the following equation:

$$\text{Suppression ratio}\,(\%) = [(A_0 - A_i)/(A_0)] \times 100\ \%$$

where A_i = the absorbance in the presence of the test compound and A_0 = the absorbance in its absence.

The ABTS (2,20-azino-bis(3-ethylbenzothiazoline-6-sulfonic acid)) radical scavenging activities of the test compounds were studied according to the following procedure [20]. ABTS was dissolved in 10 ml of double-distilled water at a concentration of 0.22 mM, and cationic radical was produced by reacting with 10 ml of 0.2623 mM potassium persulfate for 12 h in the dark. The resulting solution was diluted with phosphate buffer (pH 6) until the absorbance was 0.70 ± 0.02 at 737 nm. The reaction mixture containing 2.5 ml of ABTS solution and 0.5 ml of the test compound solution was incubated at 37 °C for 30 min in the dark. The absorbance was then measured at 737 nm (A_i, A_0). The suppression ratio was calculated according to the following equation:

$$\text{Suppression ratio}\,(\%) = [(1-A_i)/(A_0) \times 100\ \%$$

where A_i is the absorbance measured after addition of the sample and A_0 is the absorbance of the uninhibited radical cations.

For each of the above assays, the antioxidant activity is given as the 50 % inhibitory concentration (IC_{50}) [21].

Antimicrobial assays

The antibacterial activities of the compounds were evaluated against *Bacillus subtilis* and *Staphylococcus aureus* (Gram-positive) and *Escherichia coli* and *Proteus vulgaris* (Gram-negative) by the filter paper diffusion method [22]. Each test compound was dissolved in DMSO. Under aseptic conditions, circular filter papers (6.0 mm in diameter) were immersed in test solutions of different concentrations for 2 h. The filter papers were then drained off and pasted onto a Petri plate containing the bacterial suspension. The Petri plates were incubated at 37 °C for 24 h. The antimicrobial activity was evaluated by measuring the zone of growth inhibition against the test microorganisms.

Results and discussion

Crystal structure of $[Ni(L)_2]$ (1)

Single-crystal X-ray diffraction analysis reveals that complex **1** crystallizes in the monoclinic space group *C2/c*. The asymmetric unit contains one Ni^{2+} center and two L^- ligands. As shown in Fig. 1a, the nickel is six-coordinated by six nitrogen atoms from two deprotonated ligands, in which N1 from the pyrimidine ring, N4 from the imino backbone, and N5 from the pyrazine ring provide an octahedral coordination geometry. As shown in Fig. 1b, the zero-dimensional structure of **1** leads to a 1D chain structure by means of hydrogen bonds involving the chlorine atoms. The hydrogen bond distance (C–Cl···H) is 2.8625(16) Å, and the angle (C–H···Cl) is 179.41 (35)°.

Structure of $\{[Co(L)(HL)]CoCl_4\}$ (2)

X-ray diffraction analysis shows that complex **2** crystallizes in the monoclinic space group *C2/c*. As depicted in Fig. 2, the two ligands are each coordinated to the Co1 center through one imide, one pyrimidine, and one pyrazine nitrogen donors to form an octahedral cation. A tetrahedral $[CoCl_4]^{2-}$ anion maintains electroneutrality in this case.

Structures of $[Zn(L)_2]$ (3) and $\{[Ni(L)_2](H_2O)\}$ (4)

Complex **3** crystallizes in the triclinic space group $P\bar{1}$. As presented in Fig. 3, the metal atom is coordinated by two tridentate L^- ligands, leading to a distorted octahedral geometry. Complex **4** crystallizes in the monoclinic crystal system of the $P2_1/n$ space group. The asymmetric unit (Fig. S5) is composed of one independent Ni^{2+} ion, two terdentate L^- ligands, and one water ligand.

Crystal structure of $\{[Co(L)_2](NO_3)\}$ (5)

The single-crystal X-ray diffraction study reveals that complex **5** crystallizes in the triclinic space group $P\bar{1}$. As shown in Fig. S6, the metal atom is coordinated by two tridentate ligands, forming an octahedral cation, and the nitrate counterion is not coordinated. The metal–nitrogen bond lengths range from 1.8784(34) to 1.9411(33) Å and are significantly shorter than for complexes **1**, **3,** and **4,** due to the decreased ionic radius and electrophilicity of Co^{III} compared to Co^{II}. One nitrate counterion was found in the asymmetric unit, consistent with the oxidation of Co^{II} to Co^{III} [26]. This is further verified by the Co–N bond distances, which fall in the range reported for Co^{III}–N, compared to significantly longer distances for the divalent state [23–26]. The bond lengths are shortest for the metal–imino nitrogen atoms N4 and N3 and longest for the metal–pyridine nitrogen atoms N2 and N9. The same trends are also found for complexes **1**–**4**.

PXRD and thermal analyses of the complexes

In order to confirm the phrase purities of the complexes, PXRD experiments have been performed. As shown in

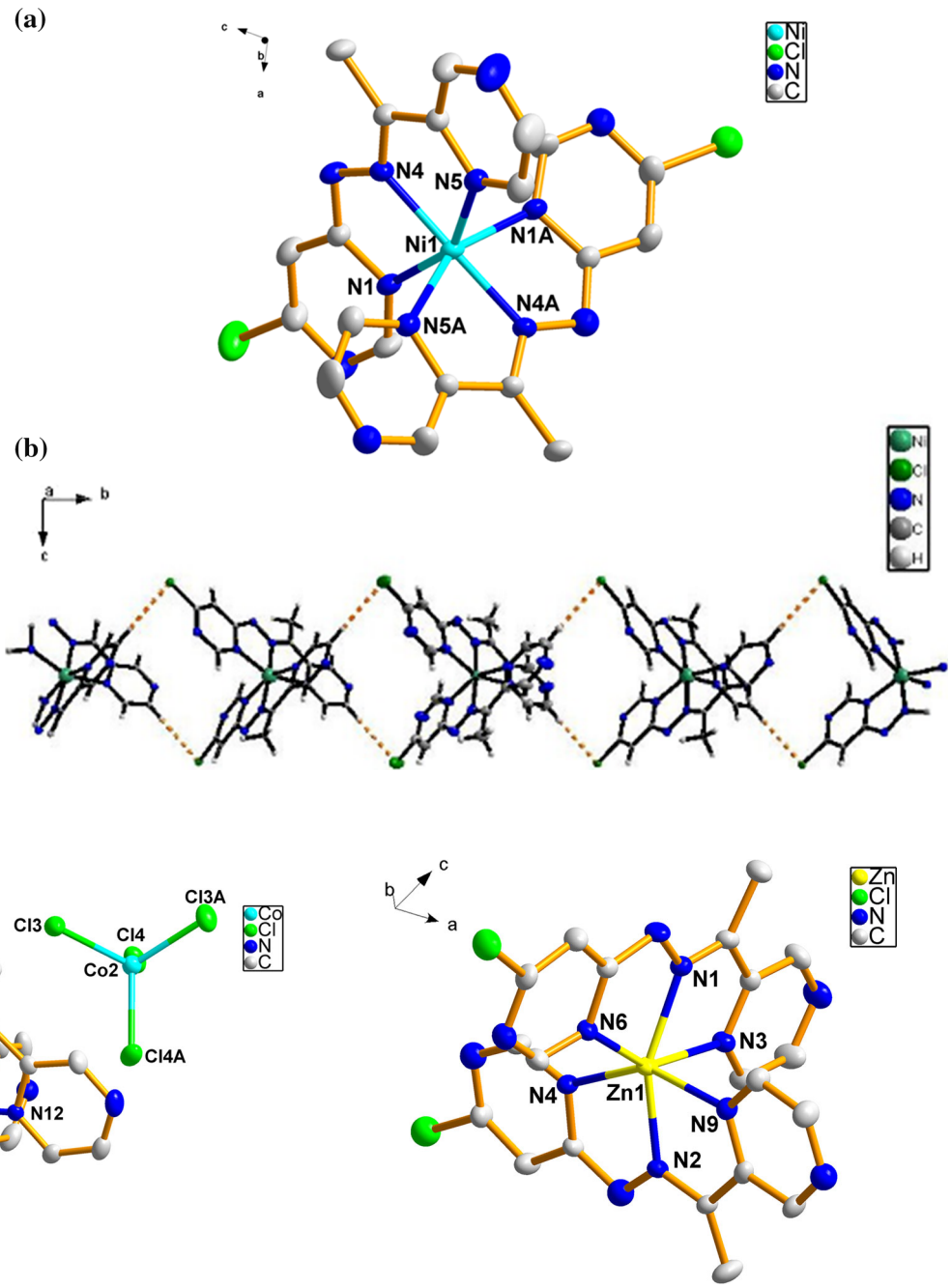

Fig. 1 **a** Crystal structure of complex **1** with 30 % thermal ellipsoids probability (symmetry code: $A = 1 - x, y, 0.5 - z$). All hydrogen atoms are ignored for clarity. **b** The 1D chain structure of complex **1**

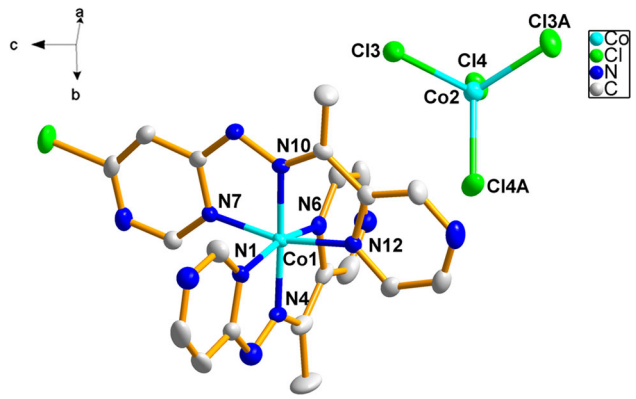

Fig. 2 Crystal structure of complex **2** with 30 % thermal ellipsoids probability (symmetry code: $A = 1 - x, y, 0.5 - z$). All hydrogen atoms are ignored for clarity

Fig. 3 Crystal structure of complex **3** with 30 % thermal ellipsoids probability. All hydrogen atoms are ignored for clarity

Fig. S7, there are good agreements between the simulated and experimental patterns, confirming the phase purities of the bulk samples. Because of the preferred orientations of the powder samples, different intensities are observed.

The thermal stabilities of the complexes have been investigated under nitrogen. As shown in Fig. S8, complexes **1–5** all exhibit similar thermal stability curves in the temperature range from 20 to 800 °C. Complex **1** undergoes a 15.66 % weight loss in the range of 321–335 °C, which may be ascribed to the loss of organic components. The residue is then stable up to 335 °C, after which decomposition is continuous. Complex **2** has excellent thermal stability, showing no weight loss until 332 °C, after which decomposition occurs. Complex **3** displays weight losses of 8.57 and 4.7 % between 184–197 and 299–311 °C, respectively. Complex **4** shows a weight loss of 2.2 % between 139 and 251 °C, which may be assigned to the departure of the water ligand, followed by

decomposition above 310 °C. Finally, complex **5** shows the onset of decomposition at 287 °C.

DPPH radical scavenging activity

The DPPH radical scavenging experiment is extensively used to assess the antioxidant properties of test compounds. The DPPH radical is relatively stable, but in the presence of a compound capable of donating hydrogen atoms, the radical is destroyed leading to a color change from purple to yellow. As shown in Fig. 4, the inhibitory effects of the test compounds on DPPH radical are concentration-related such that the suppression ratio increases with increasing sample concentration. The IC_{50} values of HL and complexes **1–5** against DPPH radicals are 24.75, 18.72, 9.32, 15.74, 20.60, and 10.27 μM, respectively, showing that the complexes have better DPPH radical scavenging activity than free HL. The Co(III) complex shows the highest scavenging effect of all.

Hydroxyl radical scavenging activity

Figure 5 compares the inhibitory effects of HL and its metal complexes on ·OH radicals. Here also, the suppression ratio of the test compounds increases with concentration. The IC_{50} values for HL and complexes **1–5** are 29.48, 15.66, 5.75, 9.64, 13.09, and 6.19 μM, respectively. As before, the Co(III) complex has the highest scavenging activity.

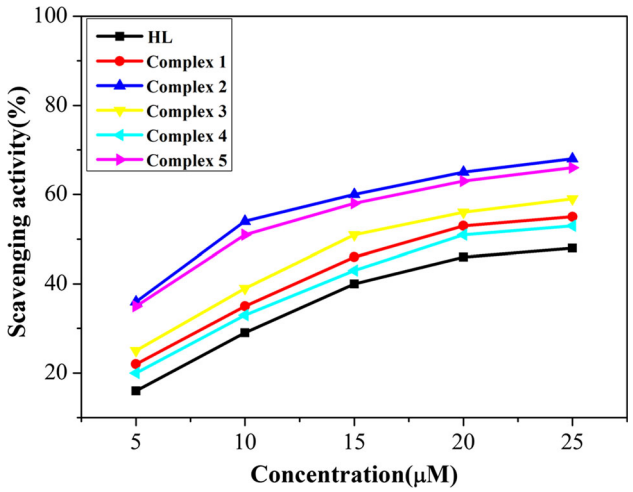

Fig. 4 Scavenging effects of HL and complexes **1–5** on DPPH radicals

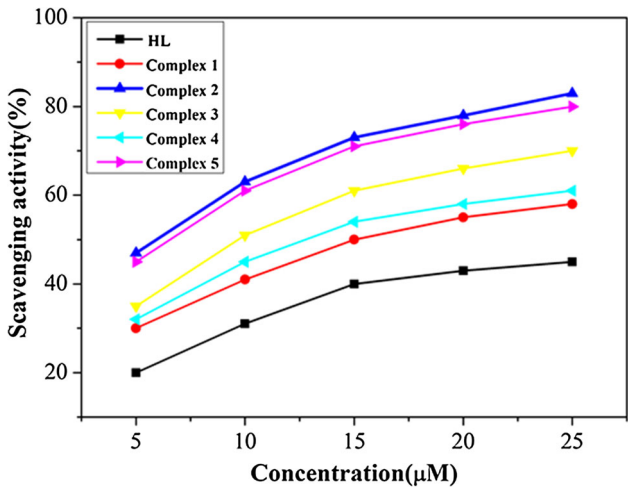

Fig. 5 Scavenging effects of HL and complexes **1–5** on ·OH radicals

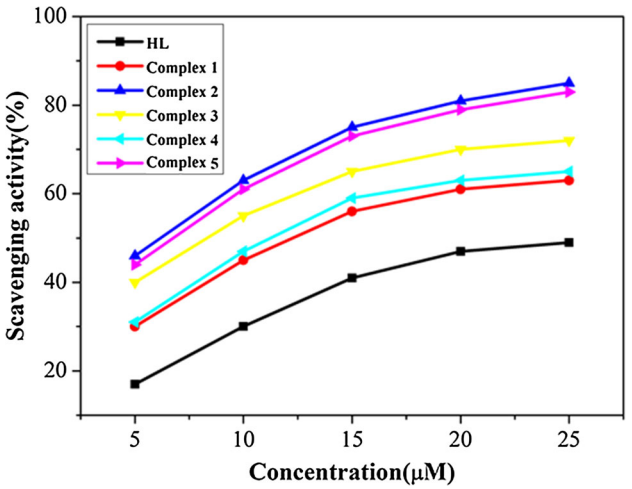

Fig. 6 Scavenging effects of HL and complexes **1–5** on $O_2^{\cdot-}$ radicals

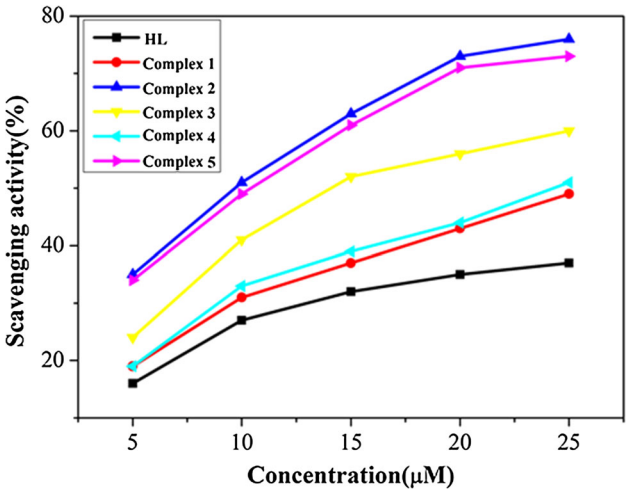

Fig. 7 Scavenging effects of HL and complexes **1–5** on ABTS radicals

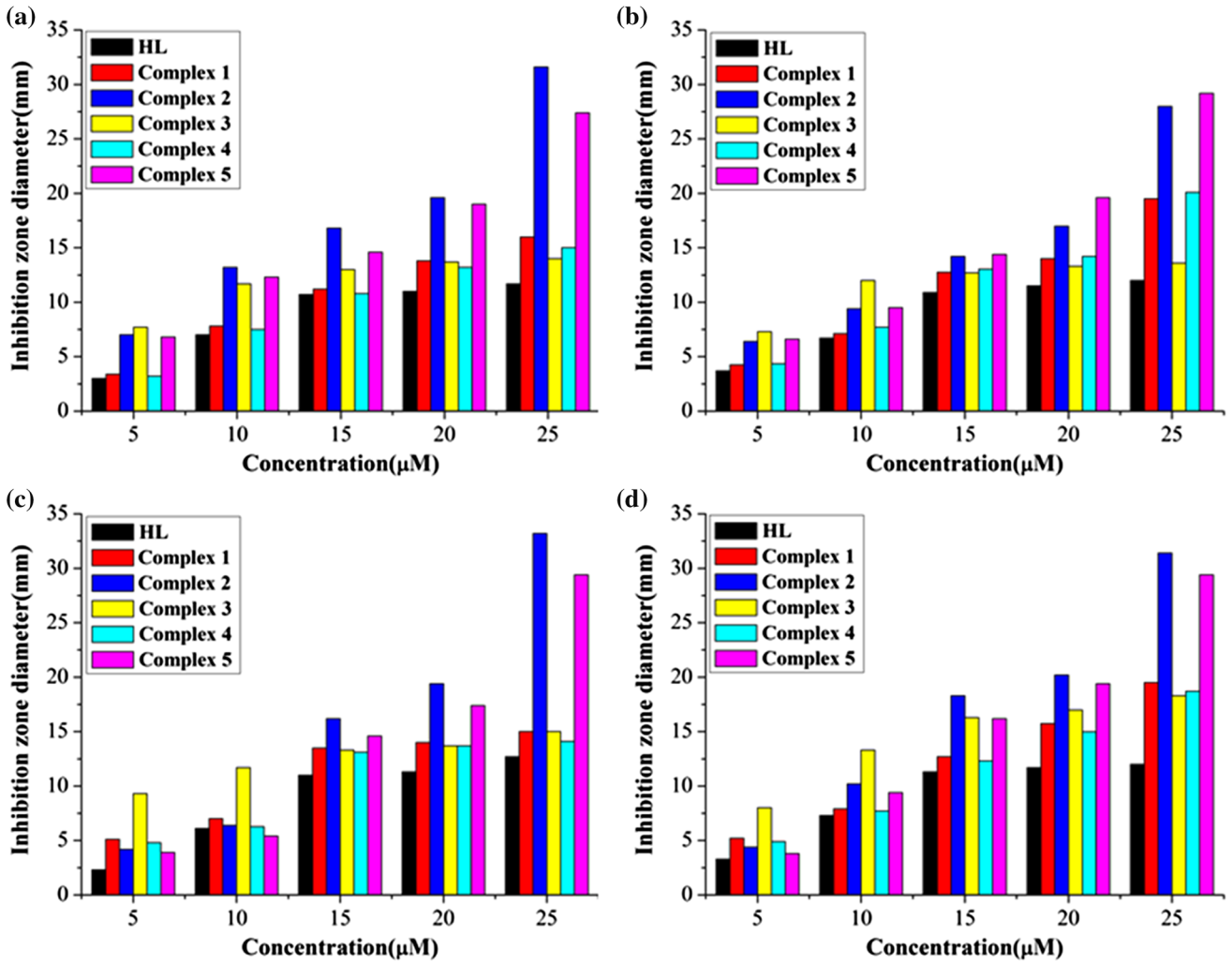

Fig. 8 Antimicrobial effects of HL and complexes **1–5** on *Escherichia coli* (**a**), *Staphylococcus aureus* (**b**), *Proteus vulgaris* (**c**), and *Bacillus subtilis* (**d**)

Superoxide anion scavenging activity

The superoxide anion scavenging activities of the test compounds are shown in Fig. 6. The IC_{50} values for free HL and complexes **1–5** are 23.66, 12.50, 5.93, 7.84, 11.41, and 6.36 μM, respectively, showing that the complexes are again more active than free HL.

ABTS radical scavenging activity

The ABTS radical scavenging experiment is usually used to evaluate the total antioxidant properties of a compound. As shown in Fig. 7, the suppression ratio of HL (IC_{50} = 49.63 μM) is the least of all these compounds, while complexes **2** and **5** (IC_{50} values for **2** and **5** are 9.03 and 9.65 μM, respectively) are more effective than the other complexes (IC_{50} values for **1**, **3,** and **4** are 27.01, 15.27, and 24.61 μM, respectively).

In vitro antibacterial activities

The antibacterial activities of free HL and its complexes are shown in Fig. 8. The antibacterial effects against all for bacteria are concentration-related such that the inhibition zone diameter increases with increasing sample concentration. Complexes **2** and **5** were found to have the highest antibacterial effects, compared to the other complexes and free HL.

Conclusion

A series of complexes based on a Schiff base ligand, 4-chloro-6-[2-(pyrazin-2-yl-methylene)hydrazinyl] pyrimidine, have been prepared and characterized. These metal complexes exhibit greater radical scavenging activities than the free Schiff base. This study may provide useful

information for the development of new antioxidants and therapeutic agents. Preliminary studies show that these complexes also possess antibacterial activities.

Acknowledgments This work was supported by grants from the Natural Science Foundation of China (Nos. 21461023 and 21361023), Fundamental Research Funds for the Gansu Universities.

References

1. Abdel Aziz AA, Elbadawy HA (2014) Spectrochim Acta A 124:404
2. Sathiyaraj S, Sampath K, Butcher RJ, Pallepogu R, Jayabalakrishnan C (2013) Eur J Med Chem 64:81
3. Suksrichavalit T, Prachayasittikul S, Nantasenamat C, Na-Ayudhya CI, Prachayasittikul V (2009) Eur J Med Chem 44:3259
4. Chen WJ, Guo P, Song J, Cao W, Bian J (2006) Bioorg Med Chem Lett 16:3582
5. Asayama S, Mizushima K, Nagaoka S, Kawakami H (2004) Bioconjugate Chem 15:1360
6. Imlay JA (2002) J Biol Inorg Chem 7:659
7. Dreher D, Junod AF (1996) Eur J Cancer 32:30
8. Dexter DT, Sian J, Rose S (1994) Ann Neurol 53:38
9. Ray PS, Maulik G, Cordis GA, Bertelli AAE, Bertelli A, Das DK (1999) Free Radical Biol Med 27:160
10. Elke F, Hasan S, Hanna GS, Dimitris AS, Reza GA (2011) Biomacromolecules 12:3528–3539
11. Satheesh CE, Raghavendra Kumar P, Sharma P, Lingaraju K, Palakshamurthy BS, Raja Naika H (2016) Inorg Chim Acta 442:1
12. Medici S, Peanaa M, Nurchi VM, Lachowicz JI, Crisponi G, Zoroddua MA (2015) Coord Chem Rev 284:329
13. Patel MN, Patel CR, Joshi HN (2013) Inorg Chem Commun 27:51
14. Raja DS, Bhuvanesh NSP, Natarajan K (2012) Dalton Trans 41:4365
15. Sathyadevi P, Krishnamoorthy P, Butorac RR, Cowley AH, Bhuvanesh NSP, Dharmaraj N (2011) Dalton Trans 40:9690
16. Nahid S, Zeinab G, Saba H (2012) Bioinorg Chem Appl 10:126451
17. Elizabeth K, Rao MNA (1990) Int J Pharm 58:237–240
18. Winterbourn CC (1981) Biochem J 198:125
19. Winterbourn CC (1979) Biochem J 182:625
20. Re R, Pellegrini N, Proteggente A, Pannala A, Yang M, Evans CR (1999) Biol Med 26:1231
21. Li Y, Yang ZY, Wu JC (2010) Eur J Med Chem 45:5692–5701
22. Liang YT, Yang GP, Liu B (2015) Dalton Trans 44:13325–13330
23. Kime NE, Ibers JA (1969) Acta Crystallogr B 25:168–169
24. Min KS, DiPasquale AG, Golen JA, Rheingold AL, Miller JS (2007) J Am Chem Soc 129:2360
25. Kil SM, Antonio GD, Arnold LR, Henry SW, Joel SM (2009) J Am Chem Soc 131:6229–6236
26. Grünwald KR, Volpe M, Cias P, Gescheidt G (2011) Inorg Chem 50:7478–7488